International Journal of Automotive Technology
https://doi.org/10.1007/s12239-024-00064-0

ELECTRIC, FUEL CELL, AND HYBRID VEHICLE, ENGINE AND EMISSIONS, HEAT TRANSFER, FLUID AND THERMAL ENGINEERING

Analysis of Power Consumption on BOP System in a Fuel Cell Electric Bus According to the Fuel Cell Load Range

Yebeen Kim[1] · Jiwoong Kim[1] · Kyoungdoug Min[1]

Received: 4 December 2023 / Revised: 22 January 2024 / Accepted: 24 January 2024

Abstract

The proton exchange membrane fuel cell (PEMFC) in a fuel cell electric bus (FCEB) converts hydrogen's chemical energy into electrical energy. The fuel cell system comprises a fuel cell stack and a balance of plant (BOP) system, which efficiently controls the stack. Fuel cell and battery are sensitive to operational temperature, which directly impacts performance, lifespan, and safety. Therefore, a thermal management system (TMS) is necessary to maintain an appropriate temperature by dissipating the heat generated by the fuel cell and battery. In this study, the exponential or quadratic relationships between the power consumption of the major components of an FCEB and various factors, such as temperature and flow rate influencing the operational behavior and control of the components, were analyzed based on the results of a dynamometer vehicle test. Additionally, the vehicle's energy flow was calculated under different fuel cell load conditions. When the fuel cell operated at 56.3 kW, TMS power was 6.6 times higher than at 20 kW. At full load, under 90 kW, it increased to 17.4 times higher. The rise in fuel cell load correlated with higher heat generation, resulting in a significant increase in power consumption for both the radiator fan and coolant pump.

Keywords Fuel cell electric bus · Proton exchange membrane fuel cell · Balance of plant system · Battery · Thermal management system · Power consumption · Operating condition

List of Symbols

C	Heat capacity, J/(kg · s)
E_{nernst}	Nernst voltage, V
E^H	Ideal voltage, 1.48 V
F	Faraday's constant, 96,485 C/mol
H	Pump head, m
I	Current, A
N	Rotational speed,
P_{dmd}	Demanded power, kW
Pr	Pressure ratio
Q_{gen}	Heat generation, kW
Q	Volumetric flow rate, L/min
R	Resistance, **Ω**
T	Temperature, K
V	Voltage, V
f_{eff}	Efficiency,
m	Mass, kg
p	Pressure, bar
v	Velocity of the fluid, m/s
z	Height of the fluid, m
ρ	Fluid density, kg/m^3
ω	Rotational speed
η	Isentropic efficiency

Subscripts

APS	Accelerator pedal sensor
BEV	Battery electric vehicle
BOP	Balance of plant
BHDC	Bi directional high voltage DC/DC converter
BLDC	Brushless direct current
BTMS	Battery thermal management system
CAN	Controller area network
COD	Cathode oxygen depletion
DC	Direct current
ECU	Electronic control unit
FC	Fuel cell
FCEB	Fuel cell electric bus
FCEV	Fuel cell electric vehicle
GDL	Gas diffusion layer
IVN	In-vehicle network

✉ Kyoungdoug Min
kdmin@snu.ac.kr

[1] Department of Mechanical Engineering, Seoul National University, Seoul 08826, Korea

Published online: 09 April 2024

MEA	Membrane electrode assembly
PE	Power electronics
PEMFC	Proton exchange membrane fuel cell
PID	Proportional integral differential
SOC	State of charge
TMS	Thermal management system
VCU	Vehicle control unit
ac	Alternating current
eff	Efficiency
is	Isentropic
ref	Reference condition

1 Introduction

Consumption of fossil fuels has been rapidly increasing due to the advancement of technology in modern society. These developments have led to significant environmental concerns, such as the depletion of energy resources, global warming caused by combustion processes, and air pollution. Prominent nations globally, particularly advanced economies, are intensifying their efforts to address these environmental issues. They are strengthening regulations on automotive exhaust emissions and focusing on power generation from clean, renewable energy sources. There has been growing interest and research in eco-friendly electric vehicles powered by fuel cells and batteries to achieve these objectives (Ahn, 2020).

A fuel cell electric vehicle (FCEV) comprises several components, including a motor, fuel cell stack, battery system, and Balance of Plant (BOP). It operates by generating electricity through electrochemical reactions between air and hydrogen. This electricity can be used to charge the battery or drive the motor. While the essential components resemble those of battery electric vehicles (BEVs), FCEVs distinguish themselves by incorporating a fuel cell stack, BOP system, and hydrogen storage facility (Choi & Choi, 2020).

A fuel cell is an energy converter that transforms the chemical energy of hydrogen into electrical energy through an electrochemical reaction. This process produces water and heat as by-products. The BOP system of a fuel cell consists of an air supply system that provides oxygen, a hydrogen supply system, and a thermal management system (TMS) that regulates the operating temperature of the fuel cell (Choi & Choi, 2020; Wang et al., 2018).

The hydrogen supply system includes an on/off valve that regulates the flow of hydrogen from the hydrogen tank to the hydrogen shut-off valve. The amount of hydrogen supplied to the fuel cell stack is controlled by adjusting the current flowing through the hydrogen supply valve. An ejector is responsible for recirculating any unreacted hydrogen by taking in a gas mixture from the stack outlet. The purge valve is a component that regulates the hydrogen concentration in the stack to a certain level. During the fuel cell reaction, water is produced and passes through the membrane due to concentration differences. It then becomes liquid in the anode and flows down to the water trap by gravity. When a certain amount of water accumulates, the drain valve opens, and the water is discharged outside. Residual air and moisture from the cathode outlet are used to humidify the dry air that flows through the humidifier and enters the cathode inlet (Choi & Choi, 2020; Wang et al., 2018).

The air supply system filters out impurities using an air cleaner and provides the necessary airflow and pressure required for the fuel cell stack reaction through an air compressor at an appropriate rate. To maintain optimal performance and durability of the fuel cell, a humidifier is used to regulate the relative humidity within the cell. The valve's opening is adjusted using an operating pressure control device to enable the pressurization of the stack, considering external air conditions (Wang et al., 2018).

The TMS is essential for controlling and maintaining the temperature of the fuel cell stack within the appropriate range, as heat is generated during the electrochemical reactions within the fuel cell stack. The cathode oxygen depletion (COD) heater, a component of the heat management system, has a dual purpose: preheating the coolant during cold starts and removing any remaining oxygen and hydrogen from the stack. The coolant is circulated by a coolant pump, and as the stack operates, it is cooled down by the radiator when the coolant temperature reaches a certain level. The ion filter plays a crucial role in the vehicle's cooling system by removing ions from the coolant. This helps regulate the electrical conductivity of the coolant, ensuring that it remains within the desired range. This, in turn, contributes to the overall stability and efficiency of the vehicle's cooling system (Kim et al., 2021; Zhao et al., 2022).

Lithium-ion batteries are widely used in electric vehicles because of their high energy density and long cycle life. However, the performance, lifespan, and safety of batteries are highly sensitive to operational temperature. Thermal runaway is a phenomenon that can lead to destructive consequences, such as the generation of gas, and even battery explosion, as the battery temperature increases rapidly. Therefore, the TMS in a battery system significantly contributes to enhancing the overall stability and efficiency of the battery system. In the battery cooling system, there is a circuit for coolant and refrigerant that helps maintain optimal operating temperatures. The coolant is responsible for transferring heat away from the battery by using a liquid cooling medium to absorb and dissipate heat. The refrigerant employs a phase-change mechanism to effectively absorb and release heat, effectively controlling the battery's temperature. The radiator in the battery TMS serves as

a crucial component in dissipating the heat generated during battery operation. It enables the transfer of thermal energy from the coolant or refrigerant to the surrounding environment, promoting effective heat dissipation in the process. The electric heater plays a vital role in cold weather conditions by providing controlled heating to prevent the battery from reaching extremely low temperatures. These components form a comprehensive cooling system that regulates temperature and addresses environmental conditions, ensuring optimal battery performance, longevity, efficiency, and safety (Kim et al., 2019).

FCEVs, which consist of fuel cell stack and batteries in a hybrid configuration, have recently gained attention for their eco-friendly and low-noise characteristics. They are also appreciated for their ability to simplify hydrogen refueling and maintenance infrastructure. The high energy density of hydrogen is crucial for increasing energy storage capacity and extending the range of vehicles, making it an optimal fuel choice for trucks, buses, and other modes of transportation. However, FCEVs often experience fluctuations in acceleration and deceleration due to their specific routes. The weight of the load fluctuates depending on the number of passengers on board the bus. The variable power demand of FCEVs can negatively affect the long-term durability of the fuel cell and battery. Various studies are currently being conducted to address this issue.

Previous literature often focuses on individual components or simple systems. Santarelli and Torchio, for instance, studied the results obtained from an experimental session aimed at characterizing the behavior of a single proton exchange membrane fuel cell (PEMFC). The research explored variations in six operational variables, including cell temperature, anode flow temperature under saturation and dry conditions, cathode flow temperature under saturation and dry conditions, and reactants pressure (Santarelli & Torchio, 2007).

Yang et al. conducted research on the development of a comprehensive transient PEMFC system model, which included the stack, membrane humidifier, electrochemical hydrogen pump, air compressor, and radiator. Rigorous validation against experimental data was performed at the subsystem level. Key findings highlighted significant performance degradation of the system at low operating current densities. Notably, the study emphasized the impact of humidifier outlet water vapor concentration, temperature, as well as air stoichiometry and temperature on the system dynamics (Yang et al., 2019).

Hou et al. focus on a fuel cell compressor and provide a comprehensive review of the air supply system. The research delved into autonomous air supply in PEMFC engines, thoroughly examining various control logics and strategies. This included single controls such as proportional integral differential (PID), model predictive, sliding mode, fuzzy, and neural, as well as hybrid or hierarchical structures like parenting, parallel, and combined (Hou et al., 2020).

In this study, the structure and operational characteristics of the main components in FCEVs were analyzed based on the results of a dynamometer vehicle test. The relationships between the power consumption of various components and factors such as coolant flow rate and temperature were examined to ensure reliable control of the system's performance. This can serve as a reference for evaluating design solutions and identifying directions for improvement in efficiency. Furthermore, the energy flow of the vehicle was calculated under different fuel cell load conditions. This calculation enables the examination of how the behavior of the fuel cell and battery system is affected and how these influences result in changes in the system's output power.

This research stands out for evaluating the entire FCEV system. The analysis not only enhances the understanding of the actual system dynamics but also establishes a foundation for optimizing the overall output power of the FCEV system. The results presented in this study make a unique contribution to the existing literature, emphasizing the significance of an experimental approach in providing insights into the performance and control strategies of FCEVs on a larger scale.

2 Analysis

Unlike general electric buses that use rechargeable electric batteries for power, FCEBs generate electricity through the operation of a fuel cell stack. Due to these characteristics, it is an efficient and eco-friendly future public transportation because it uses lightweight batteries and necessitates minimal refueling time (Alaswad et al., 2016).

Many components of FCEB are developed by directly applying existing parts of passenger cars without significant design modifications. This results in specifications and control logic that are not suitable for bus driving characteristics. In this study, an analysis was conducted to examine the relationship between various control factors and the influence of operational parameters on the performance of fuel cell and battery systems. The analysis was based on the results obtained from dynamometer vehicle experiments. It aims to predict changes in energy consumption for the BOP system of fuel cells and batteries to assist in the application of appropriate components and control strategies for FCEBs (Chu et al., 2011).

The target vehicle for the dynamometer vehicle experiment is a fuel cell electric bus (FCEB). The bus specifications include a maximum motor output of 180 kW, consisting of two 39.2 kWh batteries and two 90 kW fuel cells. The vehicle dynamometer experiments were conducted under ambient conditions, where the driving resistance

was dynamically adjusted to achieve a specific load. The resistance (R_{driving}) was continuously modified based on Eq. (1), taking into account the vehicle speed $\left(v_{\text{vehicle}}\right)$. Each coefficient was determined through measurements with f_0 and f_2. This allowed for precise control over both the load applied to the vehicle and the vehicle's speed during the experiments.

In various applications, devices such as vehicle speed sensors or steering motors are connected to electronic control units (ECUs) through shared network cables. The controller area network (CAN) protocol is widely employed in in-vehicle network (IVN) systems, including chassis network systems in the automotive industry. The increasing number of ECUs, driven by the demand for more intelligent and fuel-efficient functions, necessitates an IVN system with increased transmission capacity and reduced network delay (Kim et al., 2012).

Data for the components of FCEV were obtained using CAN, current, and voltage sensors. Power for the fuel cell, battery, and BOP components was calculated based on the current and voltage values. Additional measured data included the air compressor speed, airflow rate, inlet and outlet pressures of the air compressor, flow rate, and temperature of the coolant in the fuel cell and battery TMS, as well as the temperature of the refrigerant passing through the battery refrigerant compressor.

$$R_{\text{driving}} = f_0 + f_2 v_{\text{vehicle}}{}^2 \tag{1}$$

2.1 Fuel Cell Stack

The proton exchange membrane fuel cell (PEMFC) stack has a maximum output of 90 kW and utilizes Gore membrane electrode assembly (MEA) and SGL gas diffusion layer (GDL). Fuel cell unit cells are arranged in a series configuration to generate the demanded output (P_{stack}). In the vehicle experiment, the output voltage (V_{out}), and current (I_{out}) of the fuel cell stack are measured. The power of the fuel cell stack is calculated by multiplying the measured values using the following Eq. (2).

$$P_{\text{stack}} = V_{\text{stack}} I_{\text{stack}} \tag{2}$$

2.2 BOP System for Fuel Cell System

The fuel cell system comprises a fuel cell stack, BOP system, and TMS to efficiently control the stack as illustrated in Fig. 1. The BOP system includes an air and hydrogen supply system for providing oxygen and hydrogen, and a TMS that maintains an appropriate operational temperature range by dissipating the heat generated by the fuel cell stack. The air supply systems consist of an air cleaner, air compressor, humidifier, and control valves. The air compressor supplies air to the fuel cell stack to react at an appropriate flow rate and pressure. The humidifier supplies heat and moisture contained in the stack exhaust to the air supplied to the stack, using an internal humidifying membrane to meet the stack's requirements. The hydrogen supply system consists of a hydrogen tank, ejector, water trap, and control valves. The ejector recirculates unreacted hydrogen by drawing in the mixed gas from the stack outlet supplied by the nozzle.

The fuel cell TMS consists of a radiator, ion filter, water pump, COD heater, and control valves. The water pump circulates coolant in the fuel cell cooling system. The radiator cools the coolant from the stack, and the radiator fan is operated using an oil pressure pump. The COD heater warms up the coolant during a cold start and removes any remaining oxygen and hydrogen in the stack.

2.2.1 Air Compressor

The air compressor for the FCEB is a centrifugal compressor driven by a brushless direct current (BLDC) motor, capable of operating at a maximum speed of 100,000 RPM. It consists of a compression unit, such as an impeller or volute, and a high-speed motor. The component provides the necessary air to the fuel cell stack, ensuring an appropriate flow rate and pressure for the chemical reactions. The regulation of airflow rate depends on the motor's rotational speed, and the rapidly rotating impeller connected to the motor shaft compresses the surrounding air through its high-speed rotation. The performance of an air compressor is evaluated based on the ratio of inlet to outlet pressure and the isentropic efficiency. The flow rate and rotational speed of the compressor are determined by conducting tests under standard temperature and pressure conditions to obtain accurate values (Khanmohammadi et al., 2021).

The pressure ratio (Pr_{ac}) and isentropic efficiency (η_{ac}) of air compressor at the reference temperature (T_{ref}) and pressure (P_{ref}) can be expressed in terms of corrected flow rate ($\dot{m}_{\text{c}}$) and corrected rotational speed ($\dot{\omega}_{\text{c}}$), as shown in Eqs. (3) and (4). Since rotational speed and flow rate are influenced by temperature and pressure, the values measured under standard conditions are corrected to obtain values at standard temperature and pressure. These corrected values of rotational speed and flow rate facilitate easy comparison with values measured in different environments under the same reference conditions.

$$\text{Pr}_{\text{ac}} = \frac{p_{\text{ac,out}}}{p_{\text{ac,in}}} = f(\dot{m}_{\text{c}}, \dot{\omega}_{\text{c}}) \tag{3}$$

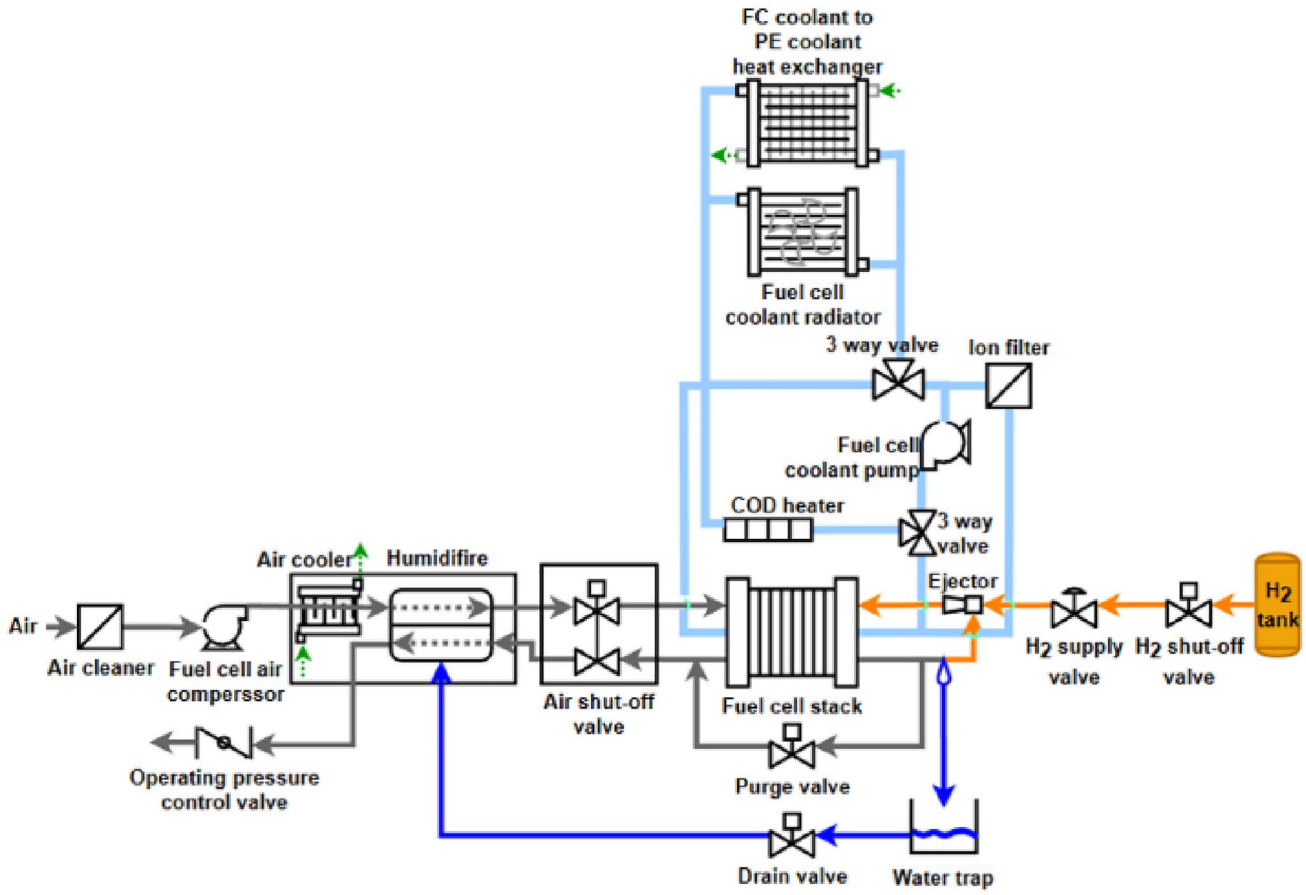

Fig. 1 Fuel cell system schematic diagram

$$\eta_{ac} = \frac{T^{is}_{ac,out} - T_{ac,in}}{T^{real}_{ac,out} - T_{ac,in}} = f(\dot{m}_c, \dot{\omega}_c) \tag{4}$$

To comprehend the control logic of the air compressor, the results of the dynamometer vehicle test were analyzed. Figures 2 and 3 illustrate the correlation between airflow and pressure downstream of the compressor, based on the stack power at different battery state of charge (SOC) levels. The relationship between stack power and air flow exhibited linearity, while the relationship between airflow and compression ratio showed a quadratic trend.

In cases of lower SOC, there is a marginal reduction in the air's lambda values, indicating a slight decrease in the ratio of the actual air supply to the required airflow for the reaction, as illustrated in Fig. 2. When BOP components, such as air compressors, need to operate initially for a fuel cell to generate electricity, and when the fuel cell uses most of its output to operate the motor, being unable to supply enough power for the BOP components of the fuel cell system, the battery operates the BOP of the fuel cell system. Therefore, in this case, if the battery SOC is low, the lambda

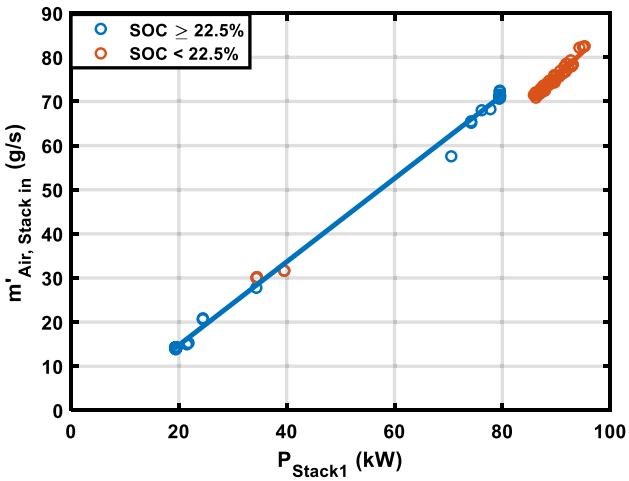

Fig. 2 Air flowrate of air compressor according to the stack power and battery SOC

of the air is kept low. In other words, there is a tendency to maintain slightly lower power consumption for the air compressor (Mwinika, 2016). Additionally, in cases of lower

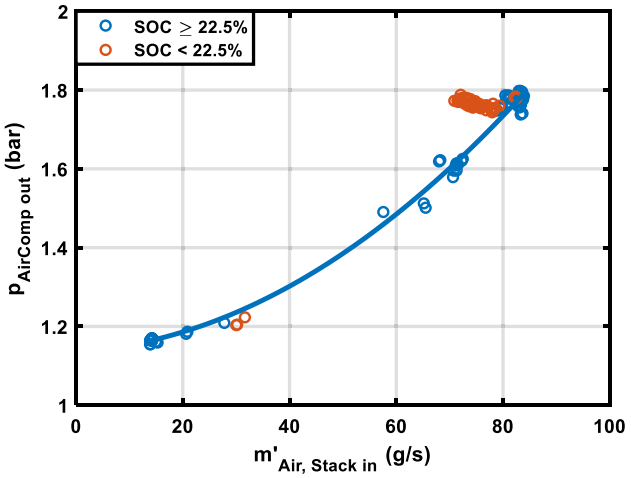

Fig. 3 Outlet pressure of air compressor according to the air flowrate and battery SOC

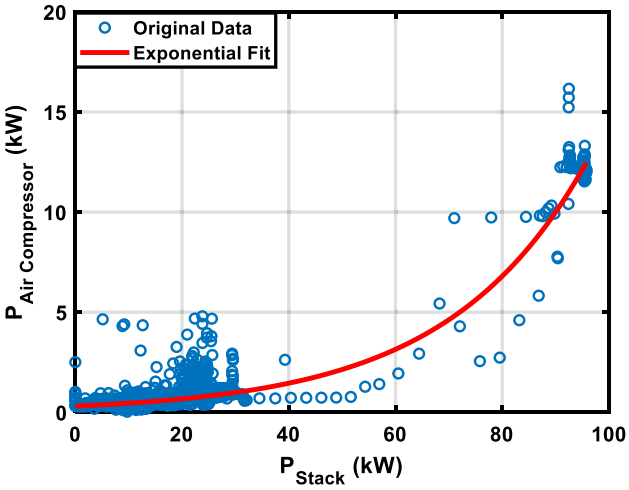

Fig. 4 Air compressor power according to the stack power

SOC, the battery might not efficiently supply power as it does in higher SOC conditions.

The fuel cell stack has to generate a higher output when the battery SOC is low to charge the battery. To improve the performance of the fuel cell stack, the compressor's compression ratio is maintained at a higher level, as shown in Fig. 3. The airflow rate is proportional to the stack current for electrochemical reactions, as shown in Eq. (5). As the current increases, the stack power also increases, leading to a corresponding rise in the required airflow rate. The air compressor operates at a higher pressure due to the larger flow rate (Rogas et al., 2017). As the desired pressure of the compressor increases, the compressor speed also rises (Bahekar & Yadav, 2014). With this increase in speed, the torque also rises, resulting in a higher air mass flow and increased power consumption of the air compressor (Yu et al., 2023). These relationships are reflected in the exponential correlation between the power of the fuel cell stack and the power consumption of the air compressor, as illustrated in Fig. 4. Therefore, assuming that the airflow rate and RPM of the air compressor are linear, the required compressor consumption power has an exponential relationship according to the required air flow rate. It indicates a rapidly growing demand for air compression to support improved electrochemical reactions within the fuel cell stack. These findings have significant implications for the design and optimization of fuel cell systems, emphasizing the importance of considering the nonlinear and exponential aspects of power dynamics.

$$\dot{m}_{\text{air}} = \frac{I_{\text{stack}}}{4F} \tag{5}$$

2.2.2 Coolant Pump

The coolant pump is an electric pump operated by an inverter, utilizing high voltage ranging from 240 to 480 V. The performance of the pump has been determined based on experimental values of coolant flow, RPM, and power obtained from vehicle tests. The temperature of the fluid is influenced by two factors: the initial temperature at the inlet and the energy input from the pump. RPM values are used as input data to control the pump. The outlet pressure and output power of a pump are expressed as shown in Eqs. (6) and (7). P_{in} refers to the inlet pressure of the pump (low-pressure) and P_{out} denotes the outlet pressure of the pump (high-pressure). Δp represents the pressure difference between the inlet and outlet of the pump. Additionally, Q is the volumetric flow rate, and f_{eff} stands for the efficiency of the pump.

$$P_{\text{out}} = P_{\text{in}} + \Delta p \tag{6}$$

$$P_{\text{mech}} = \frac{Q \cdot \Delta p}{f_{\text{eff}}} \tag{7}$$

$$0 \leq f_{\text{eff}} \leq 1 \tag{8}$$

Figure 5 illustrates the fuel cell TMS circuit, which varies according to valve openings to control the coolant flow to the radiator and heat exchanger. In this dynamometer vehicle experiment, the COD heater was not utilized because the experiment was conducted during the summer. The pressure of the pump fluid varies depending on the opening of the valve connected to the pump. As the speed of the pump increases, the pump's head (H) also increases. The increase in the pump head is expressed by the change in fluid velocity (v) and pressure (p) as shown in Eq. (9). The height of the

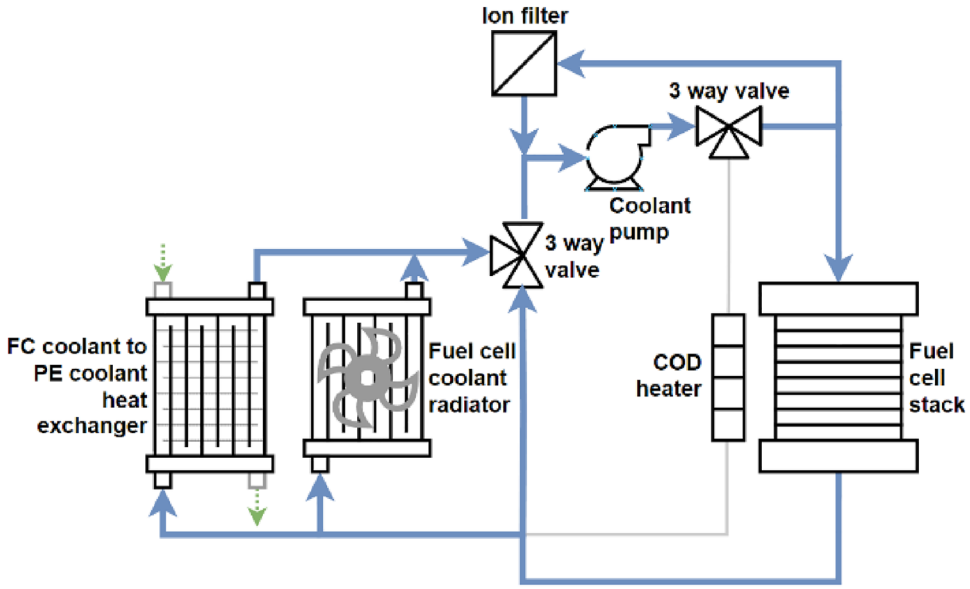

Fig. 5 FC TMS circuit not passing through the radiator

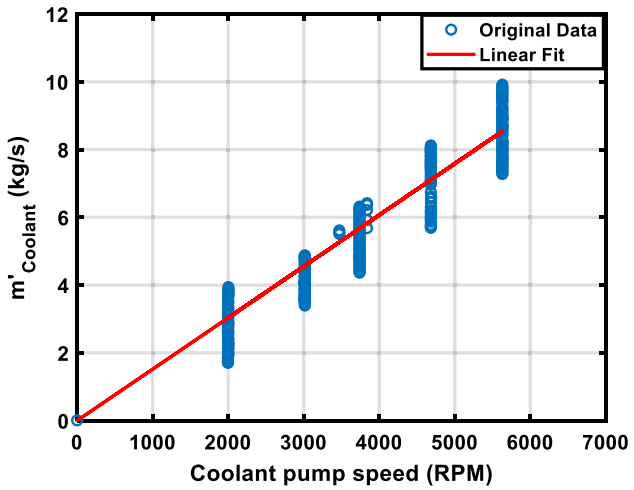

Fig. 6 Coolant pump speed according to the coolant flow rate of the coolant pump

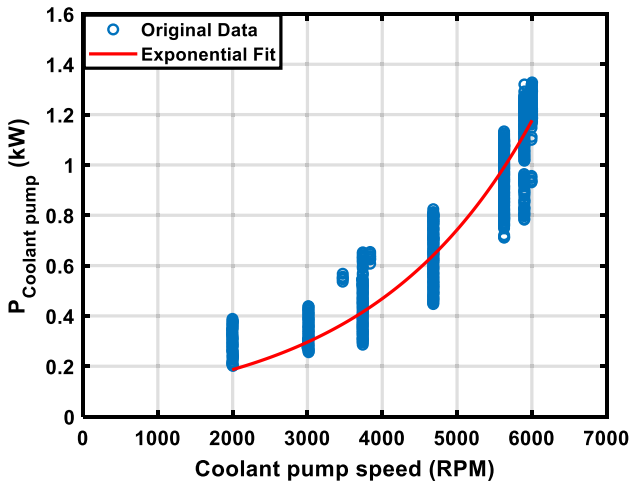

Fig. 7 Coolant pump power according to the coolant pump speed

fluid (z) can be disregarded because the pump is typically installed horizontally. As the speed of the pump increases, it transfers more energy to the fluid, resulting in an increase in the pressure difference.

In Eqs. (10) and (11), known as the affinity laws, the relationships between the coolant flowrate (Q), pump speed (N), and pump diameter (D) are defined. The coolant flow rate and pump speed exhibited a linear relationship, indicating that the flow rate varies directly with the speed. The pump speed and power (P) have an exponential correlation, suggesting that the power consumption is more sensitive to changes in pump speed, as shown in Figs. 6 and 7. The pump diameter affects the performance of the pump by influencing the coolant flow rate and power, allowing predictions of pump behavior under various operating conditions (Matlakala et al., 2019).

$$\mathrm{H} = \frac{v^2}{2g} + \frac{p}{\rho g} + z \tag{9}$$

$$Q_2 = Q_1 \left(\frac{D_2}{D_1}\right)^3 \left(\frac{N_2}{N_1}\right) \tag{10}$$

$$P_2 = P_1 \left(\frac{D_2}{D_1}\right)^5 \left(\frac{N_2}{N_1}\right)^3 \tag{11}$$

The change in coolant temperature after passing through the fuel cell is very similar to the change in stack

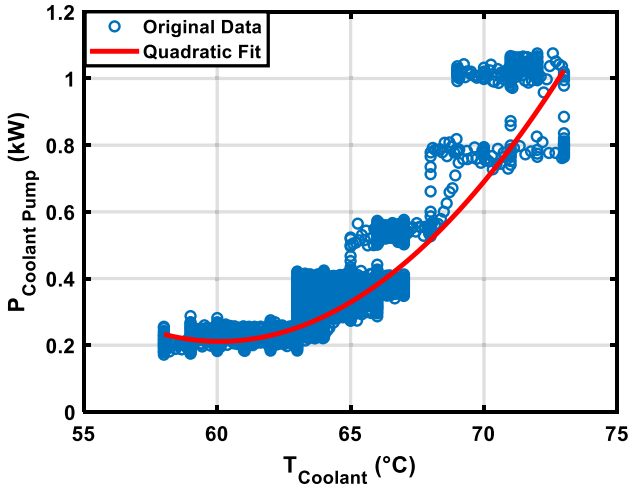

Fig. 8 Coolant pump power according to the coolant temperature of the coolant pump

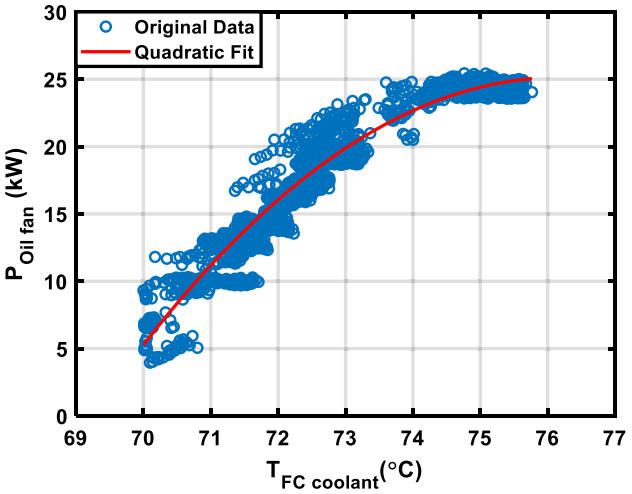

Fig. 9 Radiator fan power using an oil pressure pump according to the inlet coolant temperature of the FC radiator

temperature. As depicted in Fig. 8, there is a quadratic relationship between the coolant temperature and the power of the pump. Therefore, it is expected that the stack temperature and the power of the pump will exhibit similar quadratic trends. When the coolant temperature exceeds about 60 °C, the power consumption of the pump increases as a quadratic function. When the coolant temperature exceeds 70 °C, the pump operates at a power consumption of about 1 kW. As the stack temperature increases, the power consumption of the pump escalates rapidly. Therefore, pump power can be anticipated and controlled by adjusting coolant temperatures, leading to improved energy efficiency and extended lifespan. This approach facilitates a precise thermal management strategy, which contributes to the reliability and performance of fuel cell systems.

2.2.3 Radiator Fan Using an Oil Pressure Pump

In the FCEB's cooling system, the components of a fan, operated by an oil pressure pump, and the radiator are integrated into a single unit. The oil pressure pump uses hydraulic fluid to generate high pressure, and this pressure is utilized to rotate the fan. Therefore, the primary power for the fan is mainly supplied by the oil pressure pump. The cooling system regulates heat dissipation by adjusting the airflow generated by the fan and the coolant flow inside the radiator. The relationship between the heat dissipated by the radiator and the internal temperature variation in the stack, caused by the electrochemical reactions of oxygen and hydrogen, can be determined using Eq. (12). The flow rate of coolant passing through the radiator and the heat exchange between the coolant and the air in the radiator are control parameters used to regulate the stack temperature (Nguyen & White, 1993).

$$m_{\text{stack}} C_{\text{stack}} \frac{\mathrm{d}T_{\text{stack}}}{\mathrm{d}t} = \dot{Q}_{\text{stack,gen}} - \sum \dot{Q}_{\text{stack,out}} \tag{12}$$

$$\dot{Q}_{\text{stack,gen}} = \left(E^{\text{H}} - V_{\text{out}}\right) I_{\text{out}} \tag{13}$$

$$\sum \dot{Q}_{\text{stack,out}} = \dot{Q}_{\text{anode}} + \dot{Q}_{\text{cathode}} + \dot{Q}_{\text{coolant}} \tag{14}$$

$$\dot{Q}_{\text{coolant}} = \dot{m}_{\text{coolant}} C_{\text{p,coolant}} (T_{\text{coolant,out}} - T_{\text{coolant,in}}) \tag{15}$$

$\dot{Q}_{\text{stack,gen}}$ represents the heat generation within the stack and can be determined by multiplying the operating current (I_{out}) with the difference between the ideal voltage (E^{H}) calculated from the enthalpy of the reactions and the operating voltage (V_{out}), as expressed in Eq. (13). $\dot{Q}_{\text{anode}}$ represents the amount of heat released during the reaction where hydrogen reacts with oxygen to produce electrons and protons. Additionally, $\dot{Q}_{\text{cathode}}$ signifies the heat generated as electrons and protons combine. In other words, it represents the heat exchange at each electrode due to the chemical reaction between hydrogen and oxygen. $\dot{Q}_{\text{coolant}}$ represents the heat dissipation through forced convection heat exchange between the coolant and the fuel cell stack, as expressed in Eq. (15). It is calculated as the product of the coolant flow rate ($\dot{m}_{\text{coolant}}$), specific heat capacity ($C_{\text{p,coolant}}$), and the change in coolant temperature (T_{coolant}) as it passes through the stack.

The radiator of the FCEB is positioned on the side of the vehicle unlike conventional passenger cars. Therefore, it is speculated that the airflow impact in the radiator due to vehicle speed would be minimal. Based on vehicle test data, the control of the oil pressure pump power was analyzed for the fuel cell (FC) TMS and power electronics (PE) TMS.

In Fig. 9, when the coolant primarily flows to the radiator of the fuel cell system, with minimal flow to the PE system radiator, the power of the oil pressure pump is determined by the inlet coolant temperature of the fuel cell radiator. The oil pressure pump starts operating when the coolant temperature entering the FC radiator exceeds approximately 70 °C after passing through the stack. It operates at its maximum output of 25 kW when the coolant temperature is above approximately 73 °C. Figure 10 represents the operation of only the PE system radiator, with the fuel cell radiator not in operation. The PE system's oil pressure pump operates based on the coolant flow rate entering the PE radiator. It starts when the coolant flow rate is at or above 1 kg/s and reaches its maximum output of 25 kW when the flow rate exceeds 2.5 kg/s.

2.3 BOP System for Battery System

The battery TMS integrates both a coolant circuit and a refrigerant circuit, utilizing a liquid cooling medium and a phase-change mechanism for effective heat transfer as depicted in Fig. 11. In the coolant circuit, the coolant absorbs and dissipates the heat generated by the battery. This circuit includes a radiator, which serves as a crucial component in facilitating the transfer of thermal energy from the coolant to the surrounding environment. Additionally, an electric heater is integrated into the system to provide controlled heating during cold weather conditions, preventing the battery from reaching extremely low temperatures. The gaseous refrigerant that has passed through the evaporator in the refrigerant loop absorbs heat from the coolant as it passes through the radiator in the coolant loop. After that, the refrigerant releases heat as it passes through the

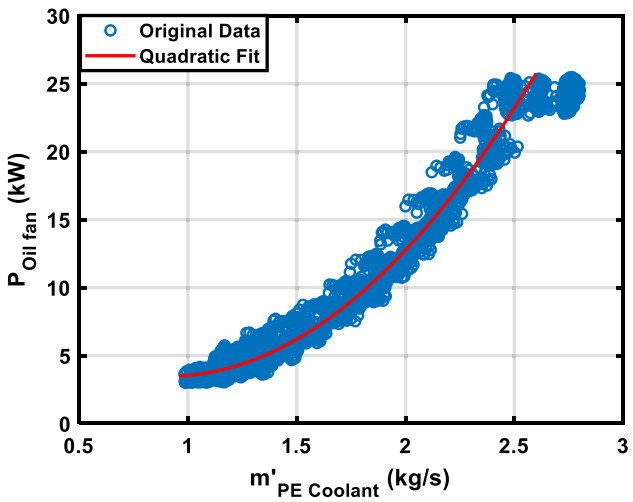

Fig. 10 Radiator fan power using an oil pressure pump according to the coolant flow rate of the PE radiator

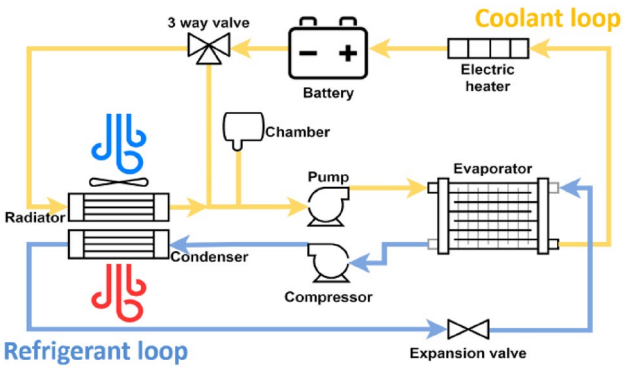

Fig. 11 Battery TMS schematic diagram

condenser and condenses to return to a liquid state. In this way, the refrigerant moves heat through repeated processes of evaporation and condensation, which results in heat exchange and temperature control in the system.

2.3.1 Refrigerant Compressor

The temperature of the battery pack is measured by the vehicle control unit (VCU) based on the battery system's signals. A battery thermal management system (BTMS) is controlled to maintain appropriate operating temperatures in the high-voltage battery system. In the BTMS, refrigerant is used to regulate the temperature of the coolant flowing through the battery. This facilitates efficient heat exchange and precise temperature control. The electric refrigerant compressor utilizes R-134a refrigerant to regulate the temperature of the cooling fluid in the high-voltage battery. It converts the fluid into a high-temperature, high-pressure gas, which is then directed to the condenser.

When the refrigerant passing through the evaporator exits at a lower temperature, the evaporator pressure decreases, and the density of the refrigerant also decreases. The refrigerant is compressed to a lesser extent when passing through the compressor at low evaporation pressure. Therefore, with lower evaporation pressure, greater energy is required to compress the refrigerant. Furthermore, the lower the density of the refrigerant, the higher the power consumption, as the compressor has to perform more work with a larger volume of gas. Consequently, at lower temperatures, the reduced density of the refrigerant demands more energy for compression. As depicted in Fig. 12, the power consumption of the refrigerant compressor tends to increase at lower refrigerant temperatures (Bolaji & Huan, 2013).

It operates at approximately 2 kW between 5 and 12 °C and decreases to 1.5 kW between 12 and 17 °C. The refrigerant temperature increases from 17 to 24 °C, compressor power decreases linearly. For refrigerant temperatures above 25 °C, the power of the refrigerant compressor is

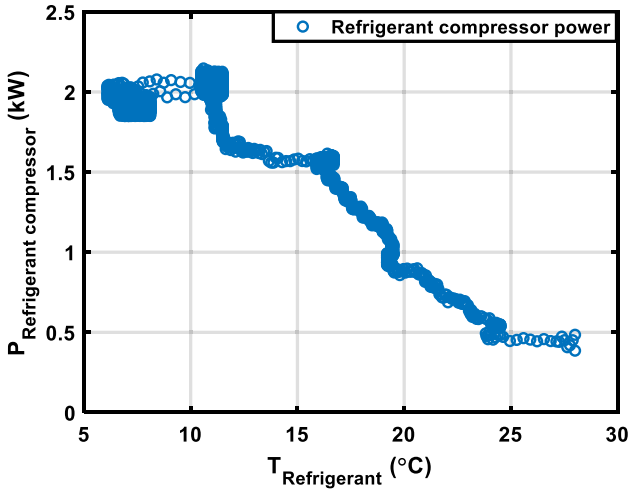

Fig. 12 Refrigerant compressor power according to the refrigerant temperature

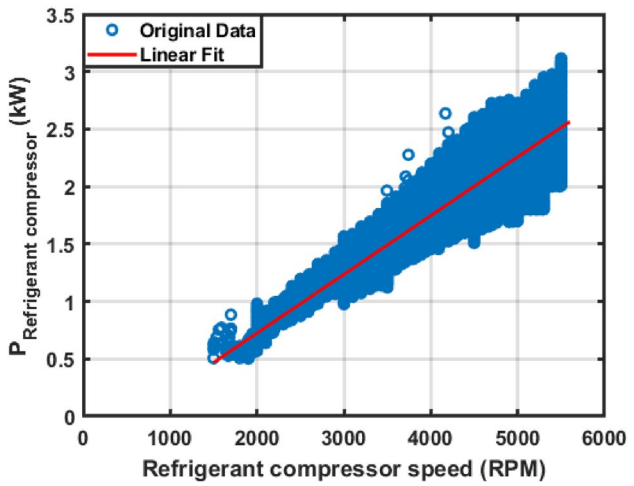

Fig. 13 Refrigerant compressor power according to the compressor RPM

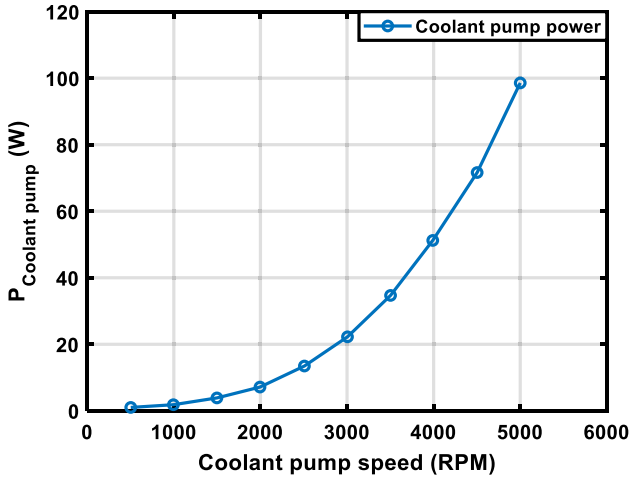

Fig. 14 Battery coolant pump power according to the coolant pump speed

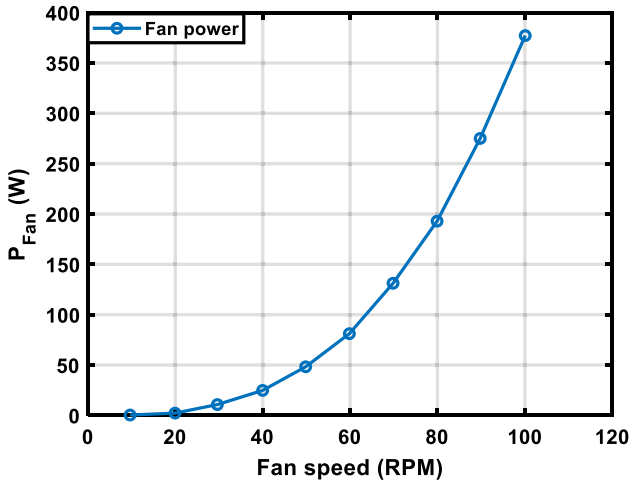

Fig. 15 Battery radiator fan power according to the fan speed

approximately 0.5 kW. Therefore, as the speed of the compressor increases, there is a tendency for the compressor power consumption to increase. However, due to variations in the refrigerant temperature, it is noted that the required power at the same compressor speed is depicted differently as observed in Fig. 13.

2.3.2 Coolant Pump & Radiator Fan

Due to the higher thermal conductivity and heat capacity of the coolant compared to the refrigerant, the coolant circuit in the BTMS allows for more efficient heat removal. As a consequence, the power consumption of the coolant pump and cooling fan of the radiator in the battery TMS is significantly lower compared to other components. Consequently, the coolant pump and radiator fan data measurements through sensors were not implemented during the dynamometer vehicle tests. Therefore, it was assumed that fan speed and fan duty followed a linear relationship. In Figs. 14 and 15, the power consumption of the coolant pump and radiator fan was calculated by applying the affinity law in Eq. (16) using Tables 1 and 2, which contain specifications of similar-scale products. The pump power (P) is proportional to the cube of the pump speed (N), denoting the maximum power ($P_{\mathrm{max,ref}}$) and speed ($N_{\mathrm{max,ref}}$) of the reference pump.

The changes in the temperature of the coolant passing through the battery are expected to follow a similar trend to the temperature of the battery. Therefore, the coolant temperature is the same as the temperature of the battery. The speed of the coolant pump is controlled based on the temperature of the battery, as shown in Fig. 16. In the temperature range of

Table 1 Specifications of coolant pump referenced

Specifications	
Model	SPAL VA33-AP91/LL-65A Metri-Pack 630 KS
Blade diameter	407 mm
Max. power	374.4W (12 V, 31.2A)

Table 2 Specifications of radiator fan referenced

Specifications	
Model	Pierburg CWA100
RPM	7000 RPM
Max. power	106.25 W
Mass flow rate	30–35 LPM (0.75 bar)/40–45 LPM (0.5 bar)

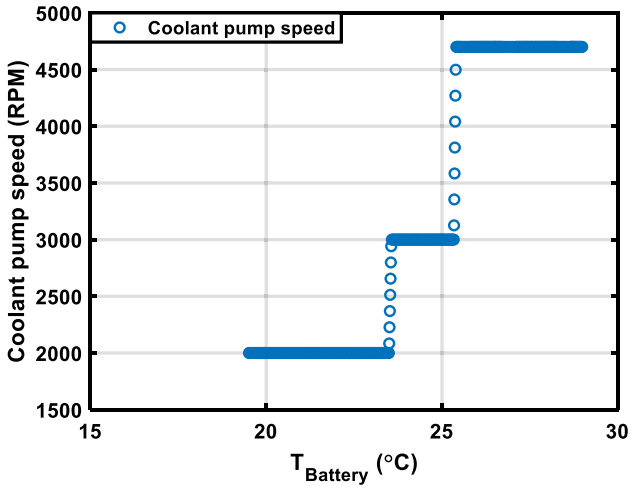

Fig. 16 Coolant pump speed according to the battery temperature

approximately 20–23 °C, the pump operates at 2000 RPM. From 23 to 26 °C, the speed of the coolant pump increases to 3000 RPM, and for temperatures exceeding 26 °C, the pump is controlled to operate at 4700 RPM.

$$P = P_{\text{max,ref}}\left(\frac{N}{N_{\text{max,ref}}}\right)^3 \tag{16}$$

3 Results

3.1 Power Consumption of FCEB

The demanded driving power is calculated based on the driving conditions, taking into account the efficiency of the driving motor. The total power demand is calculated by summing the energy required for thermal management and driving various actuators in the BOP system. It includes BOP power required for fuel supply, TMS power used to regulate the heat generated in the stack, and BTMS power used to manage the heat generated during battery operation. All of these components draw power from both the fuel cell stack and the battery, which contributes to the calculation of the total power required.

The total demanded power (P_{dmd}) consists of the power required to drive the motor ($P_{\text{motor,in}}$) and the power needed for other systems (P_{others}). They operate using power generated by both the fuel cell stack and the battery. The remaining power, except for the power necessary for the operation of the TMS and BOP system, is used to drive motors. The power generated by the fuel cell stack and battery is equal to the total output consumed by the motor, TMS and BOP system, as illustrated in Eqs. (17) and (18) (Hwang et al., 2023).

$$P_{\text{dmd}} = P_{\text{motor,in}} + P_{\text{others}} = P_{\text{stack,out}} + P_{\text{batt,out}} \tag{17}$$

$$P_{\text{others}} = P_{\text{stack,BOP}} + P_{\text{stack,TMS}} + P_{\text{batt,TMS}} + P_{\text{loss}} \tag{18}$$

There are various components that consumed power in the fuel cell system, including the air compressor and coolant pump. The BOP system of the fuel cell system is powered by the fuel cell stack, while the battery BOP system and the oil pressure pump are supplied with power from the high-voltage battery pack as shown in Fig. 16. If the power generated from the fuel cell stack is insufficient to drive the BOP components in the fuel cell system, the bi-directional high voltage DC/DC converter (BHDC) compensates by drawing power from the battery. If additional power is needed for the battery system, the power generated by the fuel cell stack is also utilized. Therefore, it is crucial to understand the variations in the output and power consumption levels of each system.

The power consumption of each BOP system in FCEBs was calculated using the current and voltage sensor measurement data obtained from dynamometer vehicle tests. In the case of an air compressor, the power consumption tends to be proportional to the required power of the stack. As the power requirement of the stack increases, the power consumption of the coolant pump and radiator in the TMS also tends to increase to maintain the optimal operating temperature of the stack.

Within the FCEB, there are two fuel cell stacks and two batteries. Since the BOP system of the fuel cell also exists in each fuel cell stack, there are two air compressors and two stack coolant pumps, as shown in Fig. 17. Although these components may not always produce completely the same output values, it is assumed that identical components will have the same output power for convenience.

3.2 Low-Load Range of the Fuel Cell Stack (19.4 kW)

The operating range, where the stack output is about 19.4 kW, is considered a relatively low-load section. In this scenario, 55% of the power is supplied by the stack, and the remaining 45% comes from the battery, which is subsequently distributed to both the motor and the BOP system. The primary power-consuming components in each system are the air compressor in the fuel cell system and the refrigerant compressor in the BTMS. Since the fuel cell stack does not require high power, the coolant pump or the oil pressure pump for the radiator also have low power requirements.

In the case of the battery system, as power is continuously drawn from the battery, the temperature of the battery increases due to the heat generated during battery discharge. The refrigerant compressor in the BTMS requires a relatively large amount of power compared to the BOP components for fuel cell stack. The results of the energy flow analysis can be seen in Fig. 18 and Table 3.

3.3 High-Load Range of the Fuel Cell Stack (56.3 kW)

Under the high-load range of the fuel cell stacks, the fuel cell stacks generate higher power than the motor. This is

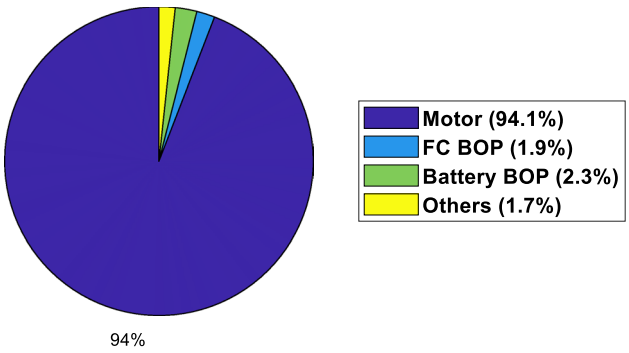

Fig. 18 Energy flow diagram (FC stack power 19.4 kW)

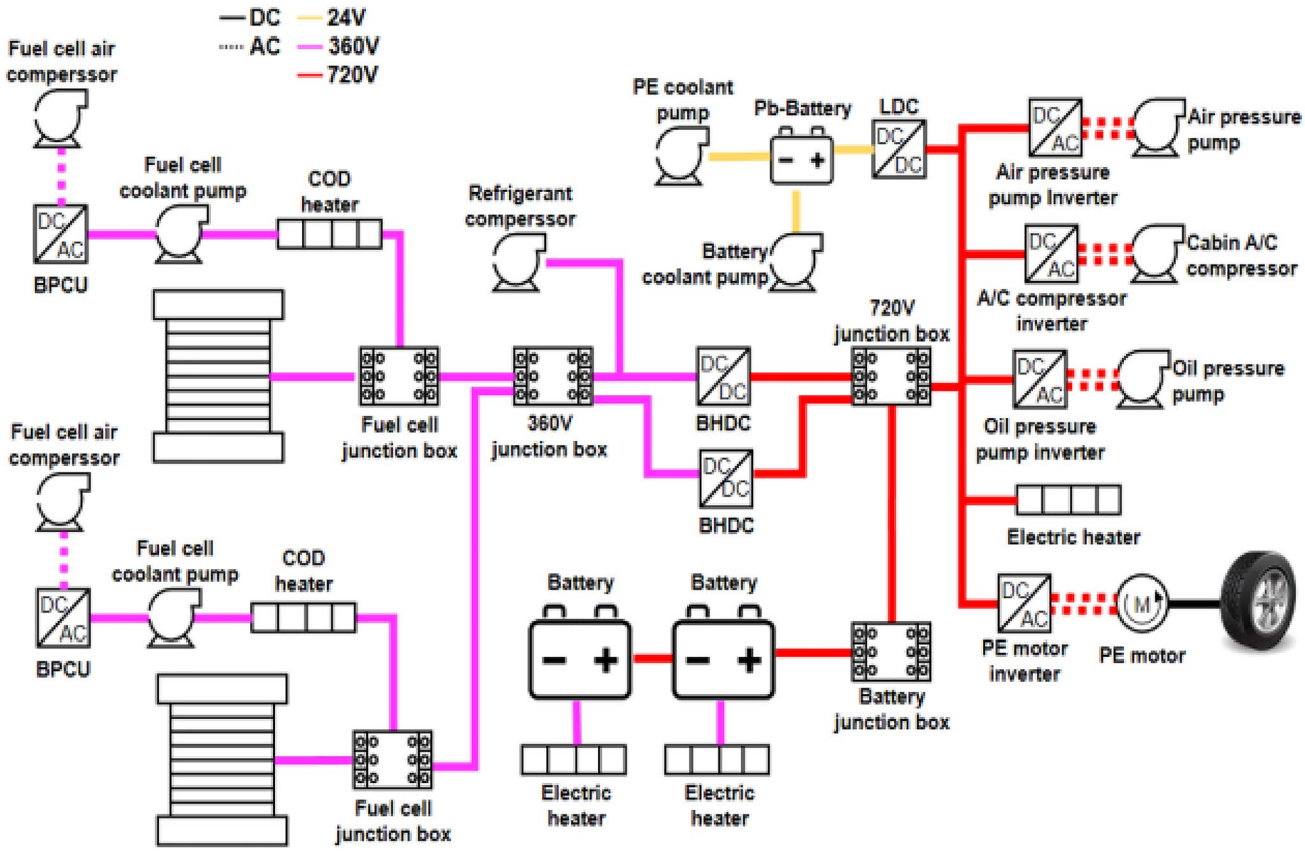

Fig. 17 FCEB's vehicle electrical system diagram

Table 3 FCEB energy flow (FC stack 19.4 kW)

	Power (kW)		Percent (%)
Stack	38.8	70.3	100
Battery	31.5		
Motor	65.9		93.7
FC compressor	0.56		0.79
FC coolant pump	0.35		0.50
FC radiator fan	0.43		0.61
Batt refrigerant compressor	1.55		2.20
Batt radiator fan	0.02		0.025
Batt coolant pump	0.01		0.028
Others	1.18		1.68

Table 4 FCEB energy flow (FC stack 56.3 kW)

	Power (kW)		Percent (%)
Stack	112.6	76.3	100
Battery	−36.3		
Motor	65.6		86
FC compressor	3.01		3.95
FC coolant pump	0.63		0.83
FC radiator fan	4.53		5.93
Batt refrigerant compressor	1.52		2.32
Batt radiator fan	0.08		0.1
Batt coolant pump	0.01		0.013
Others	0.92		1.21

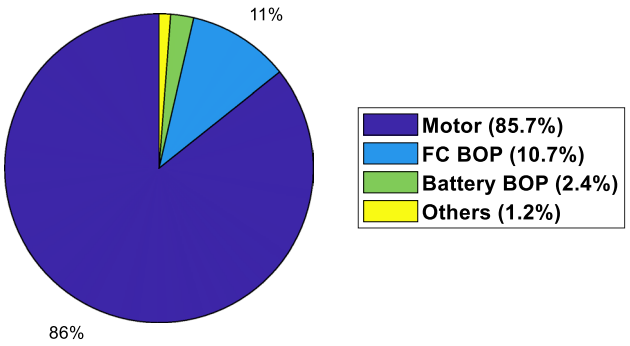

Fig. 19 Energy flow diagram (FC stack power 56.3 kW)

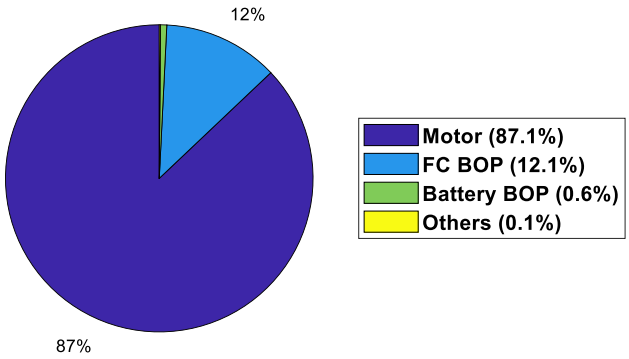

Fig. 20 Energy flow diagram (FC stack power 90.0 kW)

because the fuel cell stacks needed more power to charge the battery. An analysis of the battery pack's SOC revealed that it started at 40.4% and dropped to 35.5% after 680 s into the test. By the end of the test, it was charged back to approximately 40%. As stack power increases, the amount of heat energy generated by the stack also increases, leading to higher power consumption in the cooling system. The stack coolant pump's power consumption increased by about 1.8 times compared to the 19.4 kW section, resulting in increased heat dissipation requirements. This led to an increase in the operating speed of the radiator fan in the oil pressure pump, ultimately causing power consumption to increase by about 10.5 times compared to the 19.4 kW section. As a portion of the stack power is charged to the battery pack, the battery pack's temperature increases. It is important to note that a comparable amount of power is necessary during the discharging process. The results of the energy flow analysis can be seen in Fig. 19 and Table 4.

3.4 Full-Load Range of the Fuel Cell Stack (90.0 kW)

To operate the motor at maximum power, the fuel cell and battery are used alternately. This aims to maintain optimal operating temperatures for both the fuel cell and the battery to enhance performance. The components of the BOP system that consume the most power are the radiator fan using the oil pressure pump, radiator, and air compressor. With the increase in stack power, the heat generated by the stack also increases, resulting in higher power consumption by the components of the cooling system. The coolant pump operates at its maximum RPM within its operating range, effectively dissipating a significant amount of heat to the surrounding environment through the radiator fan. In particular, the fuel cell radiator fan showed a significant increase compared to when the power of the fuel cell was 56.3 kW. While the power consumption of the BTMS remains at a similar level to the partial load condition, the percentage of BTMS power consumption is reduced due to the significant increase in power consumed by the FC TMS. The results of the energy flow analysis are shown in Fig. 20 and Table 5.

4 Conclusion

In this study, the relationship between the power consumption of the major components of FCEB were examined. The various factors influencing the operational behavior and control of these components were analyzed. This analysis

Table 5 FCEB energy flow (FC stack 90.0 kW)

	Power (kW)		Percent (%)
Stack	180	206.9	100
Battery	26.9		
Motor	180		87
FC compressor	11.5		5.56
FC coolant pump	1.08		0.52
FC radiator fan	12.5		6.04
Batt refrigerant compressor	1.26		0.61
Batt radiator fan	0.07		0.034
Batt coolant pump	0.01		0.005
Others	0.28		0.135

was based on the results of a dynamometer vehicle test. Additionally, the power consumption and energy flow of the vehicle were calculated under different fuel cell load conditions. The total power output of the FCEB system is determined by combining the power generated by the fuel cell stack and the power stored in the battery. Through stack power analysis, several operational regions were identified, including low-load, high-load, and full-load conditions of the fuel cell stack.

To ensure optimal performance of the fuel cell stack and battery, it is essential to consider the driving characteristics of the vehicle and design the necessary components and control logic accordingly. Through this study, it is possible to predict the effect on the behavior of the fuel cell and battery system under various environments and driving conditions, along with the resulting power consumption of the BOP system. The variation of TMS power consumption depending on the battery and stack's operating temperature was confirmed and analyzed.

(1) The power supply in the hybrid configuration of the battery and fuel cell is connected to the BHDC. The power consumption of the BOP system for the fuel cell varies depending on the battery SOC and operating conditions. Notably, changes in the air lambda values of the air compressor can affect the performance of the fuel cell stack.
(2) In the case of TMS, the power consumption of the coolant pump and radiator fan, driven by the oil pressure pump, significantly increases with the higher temperature of the fuel cell stack. Consequently, under high-load conditions of the fuel cell stack and battery, where substantial heat generation occurs, the power consumption of the TMS becomes disadvantageous from an energy efficiency perspective. Therefore, there is a need for research focused on achieving efficient cooling.
(3) The current TMS of FCEB is a system that dissipates heat generated from two fuel cell stacks to a single radiator. It will be necessary to study the most efficient method of placing radiators in the TMS for each fuel cell stack and compare it to the current methods. It is important to determine the efficient method because the power of TMS decreases significantly as the operating temperature decreases.
(4) Because the coolant has higher thermal conductivity and heat capacity compared to the refrigerant, heat can be removed more efficiently through the coolant. Therefore, the BOP components in the refrigerant loop of BTMS consumes much more power than the coolant loop. Research on the battery system needs to focus on efficient refrigerant loop performance and control to minimize power consumption.
(5) The power consumption of the coolant pump and oil pressure pump for the radiator fan in the fuel cell TMS is relatively low when the stack power is low. As the power of the stack increases, the heat generated also increases, requiring higher power consumption from the cooling system. In the high-load Sect. (56.3 kW), the stack coolant pump experiences a significant increase, leading to higher heat dissipation requirements and intensified operation of the oil pressure pump-driven radiator fan. At maximum stack power (90 kW), the coolant pump operates at its maximum RPM, effectively dissipating a substantial amount of heat through the radiator fan. Consequently, the components of the TMS, including the radiator's oil pressure pump and coolant pump, exhibit a notable increase in power consumption.

Acknowledgements This work was supported and funded by the Korea Institute of Energy Technology Evaluation and Planning (KETEP) grant funded by the Korean government (MOTIE) (20223030030010, Development and demonstration of optimized fuel-cell hybrid system technology for hydrogen bus). These funds were utilized for the conduct of the research and the preparation of this journal.

Funding Open Access funding enabled and organized by Seoul National University.

Data availability The data used in this study were collected directly by the authors through experimentation. This data can be shared on a limited basis upon request to enhance the transparency and reproducibility of the research. Researchers wishing to access the data should contact the corresponding author, [Kyoungdoug Min], at [kdmin@snu.ac.kr] to request use of the data.

Declaration

Conflict of interest All authors declare that there are no other direct financial interests related to this study.

References

Ahn, S. (2020). EU's climate change responses for transport sector: Policies on electric vehicles. *Journal of International Area Studies, 24*(4), 209–234.

Alaswad, A., Baroutaji, A., Carton, J., Makky, A. A., & Olabi, A. G. (2016). Developments in fuel cell technologies in the transport sector. *International Journal of Hydrogen Energy, 41*, 16499–16508.

Bahekar, A., & Yadav, S. (2014). Optimization of air compressor motor speed for reducing power consumption. *International Journal of Innovative Research in Advanced Engineering, 1*, 6.

Bolaji, B. O., & Huan, Z. (2013). Thermodynamic analysis of the performance of a vapour compression refrigeration system, working with R290 and R600a mixtures. *Scientia Iranica, 20*, 1720–1728.

Choi, J., & Choi, J. (2020). Research status of hydrogen fuel cell system based on hydrogen electric vehicle. *Energy Engineering, 29*(4), 26–34.

Chu, K., Jo, K., Sunwoo, M., & Choi, S. (2011). Optimization of air supply for increased polymer electrolyte fuel cell system efficiency. *Transactions of the Korean Society of Automotive Engineers, 19*(3), 44–51.

Hou, J., Yang, M., Ke, C., & Zhang, J. (2020). Control logics and strategies for air supply in PEM fuel cell engines. *Applied Energy, 269*, 115059.

Hwang, G., Shin, S., Lee, S., & Kim, M. (2023). Optimal energy distribution of multi-energy sources in fuel-cell electric bus using long short-term memory. *International Journal of Automotive Technology, 24*(5), 1359–1367.

Khanmohammadi, S., Rahmani, M., Musharavati, F., Khanmohammadi, S., & Bach, Q. V. (2021). Thermal modeling and triple objective optimization of a new compressed air energy storage system integrated with rankine cycle, PEM fuel cell, and thermoelectric unit. *Journal of Sustainable Energy Technologies and Assessments, 43*, 5–7.

Kim, J., Oh, J., & Lee, H. (2019). Review on battery thermal management system for electric vehicles. *Applied Thermal Engineering, 149*, 192–212.

Kim, M., Lee, S., & Lee, K. (2012). Expanding transmission capacity of CAN systems using dual communication channels with Kalman prediction. *International Journal of Automotive Technology, 13*(2), 301–308.

Kim, S., Jeong, H., & Lee, H. (2021). Cold-start performance investigation of fuel cell electric vehicles with heat pump-assisted thermal management systems. *Energy, 232*, 121001.

Matlakala, M. E., Kallon, D. V. V., Mogapi, K. E., Mabelane, I. N., & Makgopa, D. M. (2019). Influence of impeller diameter on the performance of centrifugal pumps. *IOP Conference Series: Materials Science and Engineering, 655*, 012009.

Mwinika, T. (2016). Experimental determination of the effect of number of impeller blades on the air flow rate and power consumption of centrifugal blowers. *American Scientific Research Journal for Engineering, Technology, and Sciences, 17*, 81–88.

Nguyen, T. V., & White, R. E. (1993). A Water and heat management model for proton-exchange-membrane fuel cells. *Journal of Electrochemical Society, 140*(8), 2179–2181.

Rogas, A. C., Lopez, G. L., Aguilar, J. F. G., Alvarado, V. M., & Torres, C. L. S. (2017). Control of the air supply subsystem in a PEMFC with balance of plant simulation. *Sustainability, 9*, 73.

Santarelli, M. G., & Torchio, M. F. (2007). Experimental analysis of the effects of the operating variables on the performance of a single PEMFC. *Energy Conversion and Management, 48*, 40–51.

Wang, G., Yu, Y., Liu, H., Gong, C., Wen, S., Wang, X., & Tu, Z. (2018). Progess on design and development of polymer electrolyte membrane fuel cell systems for vehicle applications: A review. *Fuel Processing Technology, 179*, 203–228.

Yang, Z., Du, Q., Jia, Z., Yang, C., & Jiao, K. (2019). Effects of operating conditions on water and heat management by a transient multi-dimensional PEMFC system model. *Energy, 183*, 462–479.

Yu, B., Wang, F., Liu, H., Zhang, Z., & Chen, T. (2023). Research on motor rotor loss of high-speed air compressor in the application of hydrogen fuel cell vehicle. *Processes, 11*, 475.

Zhao, Y., Liu, Y., Liu, G., Li, L., & Gao, Z. (2022). Air and hydrogen supply systems and equipment for PEM fuel cells: A review. *International Journal of Green Energy, 19*(4), 203–228.